THE DISCOVERY OF ELLIPSOIDAL VARIATIONS IN THE *KEPLER* LIGHT CURVE OF

HAT-P-7

# THE DISCOVERY OF ELLIPSOIDAL VARIATIONS IN THE *KEPLER* LIGHT CURVE OF HAT-P-7

William F. Welsh[1], Jerome A. Orosz[1], Sara Seager[2], Jonathan J. Fortney[3], Jon Jenkins[4,5], Jason F. Rowe[5,6],
David Koch[5], and William J. Borucki[5]
[1] Astronomy Department, San Diego State University, San Diego, CA 92182, USA; wfw@sciences.sdsu.edu
[2] Massachusetts Institute of Technology, MA 02139, USA
[3] Department of Astronomy and Astrophysics, University of California, Santa Cruz, Santa Cruz, CA 95064, USA
[4] SETI Institute, Mountain View, CA 94043, USA
[5] NASA Ames Research Center, Moffett Field, CA 94035, USA
*Received 2009 November 15; accepted 2010 February 4; published 2010 March 31*

## ABSTRACT

We present an analysis of the early *Kepler* observations of the previously discovered transiting planet HAT-P-7b. The light curve shows the transit of the star, the occultation of the planet, and the orbit phase-dependent light from the planet. In addition, phase-dependent light from the star is present, known as "ellipsoidal variations." The very nearby planet (only four stellar radii away) gravitationally distorts the star and results in a flux modulation twice per orbit. The ellipsoidal variations can confuse interpretation of the planetary phase curve if not self-consistently included in the modeling. We fit the light curve using the Roche potential approximation and derive improved planet and orbit parameters.

*Key words:* binaries: eclipsing – planetary systems – stars: individual (BD+47, 2846, GSC0354014027)

*Online-only material:* color figures

## 1. INTRODUCTION

*Kepler* is a reconnaissance mission to obtain time-series optical photometry of ∼150,000 stars in order to determine characteristics of Earth-size and larger extrasolar planets: frequencies, sizes, orbital distributions, and correlations with the properties of the host stars (Borucki et al. 2010). To achieve these goals, *Kepler* requires exceptional long-term photometric stability and precision (Koch et al. 2010). In addition to the discovery aspect of the mission, this unprecedented photometric capability provides exquisite observations of a host of astrophysical objects, including the previously known extrasolar planets in the *Kepler* field of view. In this Letter, we examine the early *Kepler* observations of the planet HAT-P-7b.

Discovered via the *HATNet* project, the transiting planet HAT-P-7b revolves in a tight circular orbit ($a = 0.038$ AU, $P = 2.20473$ days) around a bright ($V = 10.5$ mag) F6 star (Pál et al. 2008). The proximity to its 6350 K host star (Pál et al. 2008) means the planet is highly irradiated, resulting in very high temperatures (∼2140 K), making it an extreme pM-type planet (Fortney et al. 2008). Using observations of the Rossiter–McLaughlin effect, Narita et al. (2009) and Winn et al. (2009) find that the planet's orbital axis is extremely tilted compared to the star's spin axis, and probably even retrograde, implying an interesting formation and orbital evolution history. Additionally, the radial velocities exhibit an acceleration, suggesting the presence of another body in the system, perhaps responsible for the tilted orbit (Winn et al. 2009).

Observations of HAT-P-7 during the 10 days of commissioning of the *Kepler* photometer revealed the presence of an occultation (also known as a "secondary eclipse") as the planet passes behind the star (Borucki et al. 2009). These data also show the phase "reflected" light from the planet, a result of both scattered and thermal emission. Additional observations of HAT-P-7 have been obtained, and we present these in Section 2. In Section 3,

we describe our modeling method, with particular emphasis on the ellipsoidal variations from the star. In Section 4, we present and discuss our findings.

## 2. OBSERVATIONS

HAT-P-7 was monitored continuously for 33.5 days during the 2009 May 13–Jun 15 "Quarter 1" (Q1) epoch in short-cadence mode. The 42 *Kepler* CCDs were read out every 6 s and co-added on board to achieve approximately 1 minute sampling cadence. The photometer has no shutter, so an overscan region is used to remove the effects of smearing during readout. In 6 s exposures HAT-P-7 saturates the CCD; however, because the *Kepler* photometer is such a stable platform, this does not hamper the relative precision and superb photometry is possible. For details on the design and performance of the *Kepler* photometer, see Koch et al. (2010) and Jenkins et al. (2010).

Fifteen complete transits of HAT-P-7 were observed, and after removing 21 cosmic rays via a $+4\sigma$ rejection from a 30 minute wide running median, 49,023 measurements remained. The background-subtracted light curve exhibited a gradual drop in counts (0.13%), suspected to be due to a drift in focus coupled with a fixed extraction aperture. This trend was removed using a cubic polynomial (masking out the transits). Because we are interested in phenomena on the orbital timescale (2.2 days), we chose this modest detrending to leave in as much power as possible on orbital timescales. Fluxes were normalized at phase 0.5 (mid-occultation) because the planet is hidden at this phase and we see starlight alone. Short-timescale systematic calibration features are present (Gilliland et al. 2010), but they do not affect the analysis other than being a noise term. Uncertainties were estimated by taking the median of the rms deviations in 30 minute bins, resulting in 150 ppm per one-minute datum.

The detrended and phase-folded light curve is shown in Figure 1, where the upper panel includes our fit to the transit, and the lower panel highlights the eclipse of the planet and the phase-dependent light from the planet and star. Note that the

---

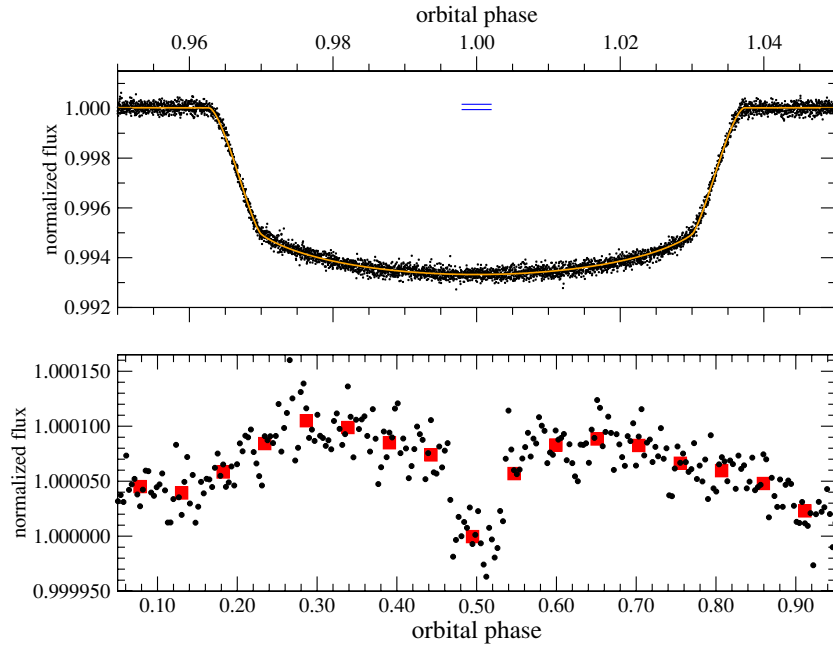[6] NASA Postdoctoral Program Fellow.

**Figure 1.** Upper: detrended and phase-folded light curve at one-minute cadence along with the ELC fit. For scale, the horizontal bars show the vertical size of the lower panel. Lower: light curve averaged in 5 minute and 75 minute bins. The double-humped shape is due to the ellipsoidal variations of the star plus light from the planet.

(A color version of this figure is available in the online journal.)

maximum does not occur just outside occultation as one would expect for simple "reflection" from the planet. Two maxima occur 0.15–0.20 away in phase, a result of the "ellipsoidal variation" of the star's light, as discussed in Section 4.

The absolute timing is still preliminary in this early version of the data calibration pipeline, but relative timing precision is reliable (though without the modest BJD correction, which is unimportant for our investigation over the 33.5 day time series). So we do not report the value for the epoch of transit T0, though of course it is a parameter in the model fitting. Also, the period measured is based only on these 33.5 days, so the precision is not as high as would be if other epochs many cycles away were included.

## 3. MODELING

We employ the ELC code of Orosz & Hauschildt (2000) to model the transit, occultation, and phase-varying light from the planet and star. The code simultaneously fits the photometry along with several observational parameters: the radial velocity $K$, and the mass and radius of the star. The $K$ amplitude was taken from Winn et al. (2009), and the mass and radius from the asteroseismology analysis of the *Kepler* data (Christensen-Dalsgaard et al. 2010). These parameters are not fixed; rather the models are started and steered toward them via a chi-square penalty for deviations. Markov chain Monte Carlo and genetic algorithms were used to search parameter space, find the global chi-square minimum, and determine confidence intervals of the fitted parameters.

The analytic model of Giménez (2006) for a spherical star and planet is not sufficient to model the phase variations. Therefore, ELC is used in its full numerical mode: the star and planet are tiled in a fine grid, and the intensity and velocity from each tile is summed to give the light curve and radial velocities. Limb and gravity darkening are included, and the gravitational distortions are modeled assuming a standard Roche potential. We employed

a blackbody approximation evaluated at a wavelength of 6000 Å, and a hybrid method[7] where model atmospheres are used to determine the intensities at the normal for each tile and a parameterized limb darkening law is used for other angles; the model is then filtered through the *Kepler* spectral response function (spanning roughly 4250–8950 Å, peaking at 5890 Å with a mean wavelength of 6400 Å; see Koch et al. 2010 and Van Cleve & Caldwell 2009). The two methods give essentially the same results, with the exception of a higher albedo from the hybrid models. Interestingly, the blackbody models yielded significantly lower chi-square values, so we quote the blackbody model values in this work. This needs to be kept in mind when interpreting the temperature and albedo estimates given in Section 4. We use a two-parameter logarithmic limb darkening law and adopt an eccentricity of zero consistent with the radial velocities and phase of occultation. We assume that the planet is tidally locked in synchronous rotation. For more details on using ELC to model exoplanet data, see Wittenmyer et al. (2005).

Following the prescription of Wilson (1990), the light from the planet is modeled as the sum of an isothermal component (with temperature $T_p$ that essentially adds a constant flux at all phases outside of occultation), and a "reflection" component on the day hemisphere. The local temperature is given by $T^4 = T_p^4 \times [1 + A_{\mathrm{bol}} \frac{F_*}{F_p}]$, which comes from assuming the fluxes and temperature are coupled by the Stefan–Boltzmann law. The bolometric albedo $A_{\mathrm{bol}}$, also known as the "heat albedo," is the ratio of re-radiated to incident energy, and should not be confused with the Bond albedo. For stars, a radiative atmosphere has $A_{\mathrm{bol}} = 1$ (local energy conservation) while for convective atmospheres a value of 0.5 is appropriate (half the energy is

---

[7] ELC can also fully employ stellar atmosphere intensities, where no parameterized limb darkening is used. But preliminary tests gave significantly worse fits unless the stellar temperature was allowed to be several thousand degrees hotter. The cause seems to be related to the very wide *Kepler* bandpass and the lack of freedom to adjust the limb darkening.

**Table 1**
HAT-P-7 System Parameters

| Parameter | Value | Uncertainty | Unit |
|---|---|---|---|
| $T_*$[a] | 6350 | $\cdots$ | K |
| $M_*$[b] | 1.53 | 0.04 | $M_\odot$ |
| $R_*$[c] | 1.98 | 0.02 | $R_\odot$ |
| $K_*$[d] | 212 | 5 | m s$^{-1}$ |
| Orbital inclination, $i$ | 83.1 | 0.5 | deg |
| Orbital period, $P$ | 2.204733 | 0.000010 | days |
| Star-to-planet radius, $R_*/R$p | 12.85 | 0.05 | |
| Limb dark coefficient $x$ | 0.58 | 0.08 | |
| Limb dark coefficient $y$ | 0.21 | 0.13 | |
| Mass of planet, $M$p | 1.82 | 0.03 | $M_J$ |
| Radius of planet, $R$p | 1.50 | 0.02 | $R_J$ |
| Semimajor axis, $a$ | 8.22 | 0.02 | $R_\odot$ |
| Bolometric (heat) albedo, $A_{bol}$ | 0.57 | 0.05 | |
| $T$p (nightside) | 2570 | 95 | K |
| $T$p (average dayside) | 2885 | 100 | K |

**Notes.**
[a] Held fixed at 6350 K; Pál et al. (2008).
[b] Steered toward $1.52 \pm 0.036$; Christensen-Dalsgaard et al. (2010).
[c] Steered toward $1.991 \pm 0.018$; Christensen-Dalsgaard et al. (2010).
[d] Steered toward $211.8 \pm 2.6$; Winn et al. (2009).

radiated, half gets redistributed; see Kallrath & Milone 1999 for a full description of the method). In our model, we allow $A_{bol}$ and the temperature ratio $T_p/T_*$ to be free parameters, keeping $T_*$ fixed at 6350 K (Pál et al. 2008). The term in brackets is the local reflection factor $\mathcal{R}$, equal to the ratio of the total radiated flux (internal + re-radiated) to internal flux. Thus $\mathcal{R} \geqslant 1$, with $\mathcal{R} = 1$ on the nightside. For an isolated planet, $T_p$ is very low (e.g., Burrows et al. 2006 assume 50 K), but for an irradiated planet, much of the incident energy is eventually re-distributed, bringing the night-time temperature up to much higher temperatures.

In the ELC model, the local emitted flux is completely dependent on the local temperature. The local temperature depends on the mean effective temperature, the local gravity, and irradiation. The irradiation term is the sum over all the visible tiles on the star as seen from each tile on the planet, and includes the ellipsoidal shape of the star, gravity darkening, limb darkening, and penumbra correction (accounting for the fact that parts of the star are not visible because they are blocked by the local horizon). Note that given the close proximity of the planet to the star, no part of the planet sees a full hemisphere of the star. There is no explicit scattering term in the reflection: the incident radiation heats up the planet and is always re-emitted locally. Scattered light is implicitly accounted for by allowing the global temperature $T_p$ to be de-coupled from the dayside temperature.

The ELC model provides a good fit to the observations. The chi square is 57,225 for 49,016 degrees of freedom (reduced $\chi_\nu^2 = 1.167$). Uncertainties on the parameters were boosted by a factor of $\sqrt{\chi_\nu^2}$ (=8%) to account for the formally high $\chi_\nu^2$, which we attribute to systematic non-Gaussian noise. The values of the parameters are listed in Table 1.

## 4. RESULTS AND DISCUSSION

The $1.8 M_J$ planet orbiting only 4.1 stellar radii from its host star induces a tidal distortion on the star, changing its shape from oblate (not spherical, due to its rotation) to a more triaxial shape, with the longest axis along the direction toward the planet

and the shortest axis perpendicular to the orbital plane.[8] This shape causes the well-known "ellipsoidal variation" effect seen in binary stars: a modulation in light at half the orbital period, with maxima at phases near 0.25 and 0.75, and unequal minima at phases 0.0 and 0.5. The ellipsoidal variation is primarily a geometrical (projected surface area) effect whose relative amplitude depends on the mass ratio and the inclination of the binary system. Given the tight constraint on the inclination from the eclipses, they may provide some limits on the mass ratio, and hence the mass of the planet. In the optical, where the phase-dependent planet-to-star flux ratio is small, the presence of the stellar ellipsoidal variation becomes significant. Neglecting its contribution can lead to a confused interpretation of the phase curve and thus an incorrect measurement of the albedo and phase-dependent scattered/thermal emission.

The presence of ellipsoidal variations in exoplanetary systems was anticipated by Loeb & Gaudi (2003) and Drake (2003), and Pfahl et al. (2008) present a detailed theoretical investigation of the tidal force on the star by the planet. Figures 1 and 3 show the first detection of the effect in an exoplanet system. In Figure 3, we show the light curve binned to 30 minutes, along with the best-fit model decomposition. The dotted curve shows the stellar-only ellipsoidal light curve while the dashed curve is the planet-only light curve (offset vertically). The solid curve is the sum of the two and equals our best-fit model. The planet-only model can match the light curve only very near phase 0.5; it is a very poor fit to the data at other phases, indicating the need for the ellipsoidal variation component. The amplitude of the ellipsoidal component is 37.3 ppm, detectable only because of *Kepler's* high-precision photometric capability.

Ellipsoidal variations arise as a consequence of gravity on a luminous fluid body. Within the Roche framework, its amplitude is exactly known if the mass ratio, inclination, orbital period, and stellar radius are known. However, since in exoplanet systems the star is not expected to be in synchronous rotation, the Roche potential is an approximation, albeit a good one since the maximum tidal distortion $\Delta R/R$ is only $10^{-4}$. However, we stress that the model presented here is only a starting point, based on the well-developed and successful Roche model. Effects such as those discussed in Pfahl et al. (2008) based on the equilibrium tide approximation can be present. As more *Kepler* data become available it will be interesting to try to distinguish between these approximations, as they can lead to measuring internal properties of the star. For example, in the frame of the rotating binary, the star is spinning retrograde if $P_{spin} > P_{orb}$, which is expected to be true for most hot Jupiter planets. This could induce a phase shift in the ellipsoidal variations, as the star's spin "drags" the tide away from the line of centers. If a phase-lag not associated with the planet light can be unambiguously measured, it may be possible to put constraints on the tidal $Q$-factor. This asymmetry could also lead to interesting orbital dynamics effects. The detailed shape and amplitude of the ellipsoidal variation also depends on the stellar envelope (convective versus radiative; Pfahl et al. 2008), thus potentially offering a probe of stellar interiors. However, for HAT-P-7, the situation is complicated by the fact that the spin axis is not aligned with the orbit axis (Winn et al. 2009), so these optimistic statements must be tempered with caution.

Figure 2 shows model light curves that illustrate the contributions of the star to the optical light. The lower curve is the

---

[8] More exactly, in a Roche potential there are four distinct radii: toward the companion, perpendicular to the orbit plane, along the direction of motion, and away from the companion.
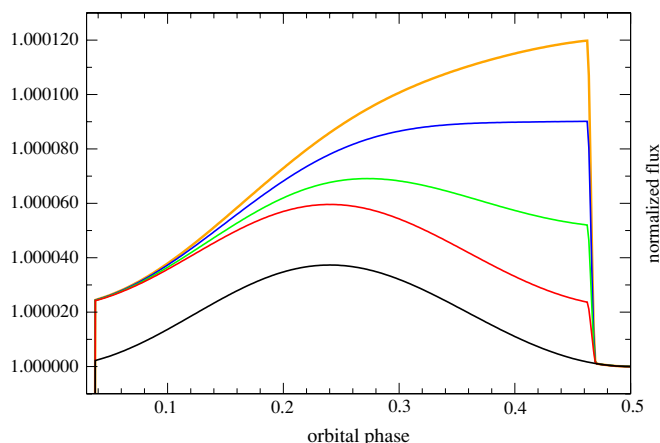
**Figure 2.** ELC model light curves for half an orbit. The bottom curve is the stellar light curve exhibiting the ellipsoidal variations. Above this are planet+star light curves with increasing bolometric (heat) albedos: 0.0, 0.3, 0.6, and 0.8. If the albedo is 0.0 the planet emits a constant amount of light resulting in a simple offset in flux. As the albedo increases, the light from the planet becomes more pronounced.

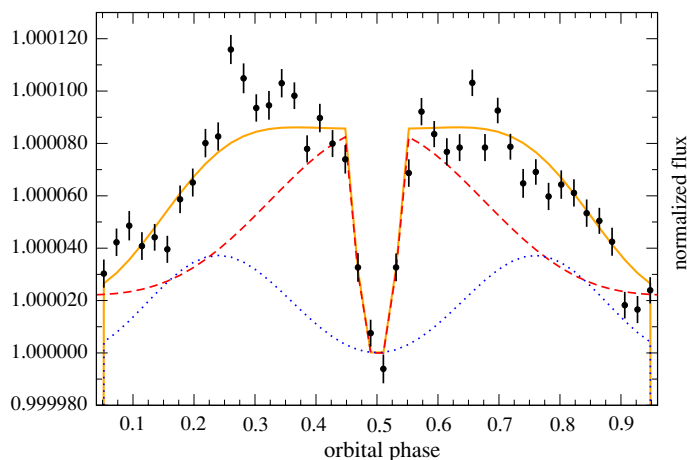(A color version of this figure is available in the online journal.)



**Figure 3.** Phase-folded *Kepler* light curve with the best-fit model (solid curve). Also shown are the component stellar-only ellipsoidal model (dotted) and the planet-only model (offset by +1; dashed). Both the data and models have been cast into 30 minute bins.

(A color version of this figure is available in the online journal.)

stellar light only, showing the ellipsoidal variations. It is not constant outside of transit, and its amplitude can be significant compared to the depth of the occultation. Above this are four curves that include the planet contribution. The lowest is for an isothermal isotropic planet with no phase-dependent scattered or re-radiated emission. To first order, it is essentially an additive offset to the star's light, the amount depending on the relative radius and temperature of the planet. If the absorbed incident energy from the star is not perfectly uniformly re-distributed around the planet, the dayside of the planet will be hotter than the nightside, resulting in an orbit-phase-dependent modulation peaking at the sub-stellar point (phase 0.5). Or, if the atmosphere scatters the incident radiation, again the dayside will be brighter than the nightside (though not necessarily hotter). The upper three curves show this phase-dependent effect for different values of the heat albedo, which is a proxy for scattered and re-radiated emission on the dayside. Note that advection can move the peak downwind and produce a phase shift in the planet's emission, as seen in the infrared phase curve of HD189733 (Knutson et al. 2007); this is not included in these models.

Given a stellar temperature estimate, the ELC model can yield day and night hemisphere temperatures. Because the planet is not black it contributes light at all phases (other than occultation) and its flux contribution at each orbital phase, relative to ellipsoidal and other effects, allows its temperature to be estimated. In particular, the ability to measure relative temperatures arises from the requirement of getting the occultation and transit depths correct given the tight geometric constraints (e.g., a 2600 K planet reduces the 6000 Å transit depth by 29 ppm compared to a zero temperature planet). We find that the peak temperature on the planet (at the sub-stellar point) is 3160 K, but a more meaningful flux-weighted day temperature is $2885 \pm 100$ K. This is notably higher than the $2560 \pm 100$ K estimate by Borucki et al. (2009). We caution that the dayside temperature estimate is derived from the assumption that the light is entirely thermal in origin with no scattered component; thus this is a maximum dayside temperature estimate for the given heat albedo. We find that the nightside temperature $T_p$ is a surprisingly hot $2570 \pm 95$ K, only 590 K less than the peak day temperature.

As seen in Figure 3, the depth of the occultation is 85.8 ppm, and the nightside contribution of the planet is 22.1 ppm, giving a dayside peak flux enhancement of 63.7 ppm. Combining these flux ratios, temperatures, and the relative radii, we can attempt to estimate the geometric and Bond albedos (see Rowe et al. 2008 for a discussion). The planet's albedo is key to the energy balance in the planetary atmosphere and its importance for the dayside emission is discussed in several papers (e.g., Seager et al. 2005; Burrows et al. 2006; Lopez-Morales & Seager 2007). The geometric albedo is given by the ratio of planet to star flux at phase 0.5, scaled by the ratio of surface areas: $A_g = (F_p/F_*)/(R_p/a)^2$. Using the peak planet to star flux of 63.7 ppm yields $A_g = 0.18$. This agrees with the $<0.20$ value found for the pM-class planet CoRoT-1b (Snellen et al. 2009; Alonso et al. 2009b), but is significantly higher than some other planets, notably $A_g < 0.08$ for HD 209458b (Rowe et al. 2006) and $0.06 \pm 0.06$ for CoRoT-2b (Alonso et al. 2009a). The equilibrium temperature and Bond albedo are related by the definition: $T_{eq}^4 = T_*^4 (R_*/2a)^2 [f(1 - A_B)]$, where $f$ is the redistribution factor and equals 1 for complete redistribution or 2 if the incident flux is re-radiated only on the day hemisphere. Setting $f = 1$ and equating the nightside temperature with the equilibrium temperature should in principle allow one to solve for the Bond albedo since all the other terms are known. However, this fails because the maximum equilibrium temperature possible (when $A_B = 0$) is 2213 K, considerably *less* than the ELC estimate. It may be that our 6000 Å brightness temperature estimate exceeds the equilibrium temperature simply because the planet is not a blackbody and at other wavelengths lower temperatures may be measured. We speculate on two other possibilities, both related to the presence of a third body in the HAT-P-7 system. First, the planet may genuinely be hotter than the equilibrium temperature due to non-radiative heating, perhaps tidal heating due to an encounter with another object (recall the $>86°$ offset between the orbit and stellar spin axes; Winn et al. 2009; Narita et al. 2009). A more mundane, but perhaps more likely, explanation is that light from a third body is contaminating the flux ratios. The acceleration term in the radial velocities suggests the presence of another body (Winn et al. 2009). When more *Kepler* transits are available, we can check for transit timing variations and address the issue of potential third light contamination.

In closing, the *Kepler* light of HAT-P-7 curve reveals ellipsoidal variations with an amplitude of approximately 37 ppm. This is the first detection of ellipsoidal variations in an exoplanet host star, and shows the precision *Kepler* is capable of producing at this early stage. For comparison, a transit of an Earth-analog planet around a Sun-like star would produce a signal depth of 84 ppm, a factor of 2 larger than this effect.

## REFERENCES

Alonso, R., et al. 2009a, A&A, 506, 353
Alonso, R., et al. 2009b, A&A, 501, L23
Borucki, W. J., et al. 2009, Science, 325, 709
Borucki, W. J., et al. 2010, Science, 327, 977
Burrows, A., Sudarsky, D., & Hubeny, I. 2006, ApJ, 650, 1140
Christensen-Dalsgaard, J., et al. 2010, ApJ, 713, L164
Drake, A. J. 2003, ApJ, 589, 1020
Fortney, J. J., Lodders, K., Marley, M., & Freedman, R. 2008, ApJ, 678, 1419
Gilliland, R., et al. 2010, PASP, submitted
Giménez, A. 2006, ApJ, 650, 408
Jenkins, J., et al. 2010, ApJ, 713, L120
Kallrath, J., & Milone, E. F. 1999, Eclipsing Binary Stars (New York: Springer)
Knutson, H. A., et al. 2007, Nature, 447, 183
Koch, D., et al. 2010, ApJ, 713, L79
Loeb, A., & Gaudi, B. S. 2003, ApJ, 588, L117
Lopez-Morales, M., & Seager, S. 2007, ApJ, 667, 191
Narita, N., Sato, B., Hirano, T., & Tamura, M. 2009, PASJ, 61, L35
Orosz, J. A., & Hauschildt, P. H. 2000, A&A, 364, 265
Pál, A., et al. 2008, ApJ, 680, 1450
Pfahl, E., Arras, P., & Paxton, B. 2008, ApJ, 679, 783
Rowe, J. F., et al. 2006, ApJ, 646, 1241
Rowe, J. F., et al. 2008, ApJ, 689, 1345
Seager, S., et al. 2005, ApJ, 632, 1122
Snellen, I. A. G., de Mooij, E. J. W., & Albrecht, S. 2009, Nature, 459, 543
Van Cleve, J., & Caldwell, D. 2009, Kepler Instrument Handbook KSCI-10933-001, NASA Ames Research Center, Moffett Field, CA (http://keplergo.arc.nasa.gov/Instrumentation.shtml)
Wilson, R. E. 1990, ApJ, 356, 613
Winn, J. N., et al. 2009, ApJ, 703, 99
Wittenmyer, R. A., et al. 2005, ApJ, 632, 1157